IEEE Access
Multidisciplinary | Rapid Review | Open Access Journal

Received 22 February 2023, accepted 12 March 2023, date of publication 27 March 2023, date of current version 30 March 2023.

Digital Object Identifier 10.1109/ACCESS.2023.3262172

RESEARCH ARTICLE

Stability Enhancement of Grid-Connected Wind Power Generation System Using PSS, SFCL and STATCOM

MUHAMMAD SARWAR[1], MUHAMMAD ARSHED[2], BABAR HUSSAIN[2], MUHAMMAD RASHEED[2], HANAN TARIQ[3], STANISLAW CZAPP[3], (Member, IEEE), SARMAD TARIQ[4,5], AND INTISAR ALI SAJJAD[5], (Member, IEEE)

[1]Department of Electrical and Computer Engineering, Iowa State University, Ames, IA 50011, USA
[2]Department of Electrical Engineering, Pakistan Institute of Engineering and Applied Sciences (PIEAS), Islamabad 45650, Pakistan
[3]Faculty of Electrical and Control Engineering, Gdańsk University of Technology, 80-233 Gdańsk, Poland
[4]National Transmission and Despatch Company, Lahore 54000, Pakistan
[5]Electrical Engineering Department, University of Engineering and Technology, Taxila, Islamabad 47050, Pakistan

Corresponding author: Stanislaw Czapp (stanislaw.czapp@pg.edu.pl)

This work was supported by the Gdańsk University of Technology.

ABSTRACT The stability related issues may occur in a power system due to disturbances in generating or loading conditions, especially in the presence of distributed generation (DG) based on renewable energy resources (RERs). This paper proposes a novel strategy for the stability enhancement of a wind power generation system (WPGS) by using a combination of three devices, namely, a power system stabilizer (PSS), resistive superconductor fault current limiter (R-SFCL) and static synchronous compensator (STATCOM). The small signal (SS) stability of the test system is enhanced by selecting the best PSS type from the different types of PSS. An R-SFCL is used for improving the rotor angle and the frequency stability of the test system. Two indices, namely, transient stability index and sum of maximum deviations (SMD) index are introduced for determining the optimal locations of different sized R-SFCLs for increasing the rotor angle stability. The sensitivity index (SI) based on the power change between areas is applied for determining the optimal locations of different sized R-SFCLs for enhancing the frequency stability. Along with rotor angle and frequency stability, LVRT capability improvement of the wind farm using STATCOM is also considered. Finally, the combined effect of R-SFCL and STATCOM on the rotor angle and the frequency stability, for different fault locations, is also investigated for determining the optimal location of an R-SFCL in the presence of STATCOM. The results presented in the paper show that STATCOM affects both the number of feasible locations and the optimal locations that can be selected for different sized R-SFCLs for augmenting the rotor angle and the frequency stability of the system during faults. Moreover, it is pointed out that an optimal combination between the different sizes and the locations of R-SFCLs and STATCOM exists to enhance the overall stability of the test system under fault conditions.

INDEX TERMS Resistive superconductor fault current limiter, stability enhancement, STATCOM, LVRT, wind energy.

I. INTRODUCTION

A power system is considered stable if it can maintain an equilibrium state when subjected to physical disturbances. Small-signal (SS) stability describes the ability of a power system to remain in synchronism mode in case of small load variations or decoupled generators. The transient stability deals with the ability of a system to maintain its stability after occurrence of a severe disturbance, i.e., faults. The stability issues may occur in a power system due to a large change in generation or loading conditions. These issues are aggravated due to large scale integration of renewable energy resources

The associate editor coordinating the review of this manuscript and approving it for publication was Akin Tascikaraoglu.

(RERs) especially based on wind power generation. Due to intermittent nature of wind power, the transient, frequency and voltage stability may be affected. Moreover, power generated from wind turbines would change the power flow of the system and have an effect on the primary oscillation modes of synchronous generators (SGs). In extreme cases, the tripping of one wind turbine may cause cascaded tripping of other subsequent wind turbines and system generators and might result into a major black out. Moreover, different types of induction generators (IGs), widely deployed in wind energy conversion systems (WECSs), may also suffer due to their high sensitivity to grid disturbances and faults [1]. Thus, it is important to devise a strategy to operate various system generators within their stability margins especially in presence of a large share of wind generation.

The use of PSS is described for damping of low frequency oscillations (LFOs) of wind power systems in [2], [3] and for enhancing the rotor angle stability of doubly fed induction generator (DFIG) based wind power systems in [4].

For the transient stability enhancement, use of braking resistors [5], [6], Superconducting Fault Current Limiters (SFCLs) [7], [8], [9], Flexible AC Transmission Systems (FACTS) devices [10], [11], [12], and Superconducting Magnetic Energy Storage (SMES) [13], [14], etc., is extensively discussed in literature. Fault Current Limiter (FCL), an active power controlling device, is very effective in improving the transient stability of a power system. Authors in [15] proposed a bridge type FCL with optimal reclosing of the circuit breaker to enhance transient stability. The use of a solid state FCL (SSFCL) for enhancing the dynamic damping of a power network with wind-turbine power generation is described in [16]. The performance of SFCL for improving the transient stability of a power system is analyzed in [17], [18]. A comparison of inductive and resistive types of an SFCL with respect to transient stability enhancement of a power system is described in [19].

In [20], optimal location of SFCL, in order to improve rotor angle stability is determined by using IEEE benchmark four machine two area test system. In that literature, transient stability index and optimal resistive values are determined on the basis of sum of maximum deviations. In [21], optimal location of SFCL to damp out low frequency oscillations is determined by using IEEE benchmark four machine two area test system. In [22], double-integral sliding mode controller (DISMC) based bridge-type flux-coupling non SFCL has been proposed to improve fault ride-through (FRT) capability and rotor angle stability response of a DFIG-based wind power system. In [23], the authors have discussed the relation between the location of SFCL and type of power system stabilizer (PSS) to enhance the transient stability.

FACTS devices including static synchronous compensator (STATCOM) have a number of applications including enhancement of transient stability and Low Voltage Ride Through (LVRT) capability. The effect of fuzzy logic controller based static var compensator and static synchronous compensator on power system stability has been studied in [24]. It is concluded by the authors that STATCOM has a better performance in respect of stability improvement of the system as compared to static Var compensator (SVC). The LVRT capability of a doubly fed induction generator (DFIG) based wind farm is enhanced with STATCOM in dynamic conditions. Metaheuristic optimization algorithms like the Water Cycle Algorithm (WCA), Particle Swarm Optimization (PSO) and a hybrid algorithm of both WCA and PSO are used to enhance the STATCOM performance [25]. The combined interaction of a unified power quality conditioner and superconducting magnetic energy storage is proposed to enhance the LVRT of DFIG and the permanent magnet synchronous generator. The effectiveness of the proposed technique is verified during fault conditions and wind speed variation [26]. Similarly, coordinated design and application of robust supplementary damping controllers for STATCOM and SVC to improve the SS stability of a large power system is described in [27]. A comprehensive review is presented in [28] to enhance LVRT and high voltage ride through for the DFIG system using different techniques including STATCOM. In [29], coordination of SSSC and PSSs controllers is proposed for improvement of transient stability and LVRT capability of a power system connected with wind and photovoltaic (PV) based generation. In [30], the application of SVC is considered to increase the voltage stability and the LVRT capability of the DFIG based wind farm system. The effect of STATCOM and SVC on dynamic voltage stability during LVRT of wind turbine systems is investigated in [31]. In [32] a nonlinear generalization of the robust coordinated PSS-AVR is proposed to enlarge the stability region and for enhancing the transients response during faults. In [33] the synergetic control (a nonlinear control method) is applied to the decentralized TCSC controller for improving transient stability and voltage regulation, and to schedule TCSC line active power transfer in a wide range of operation conditions. The rotor side crowbar circuit is proposed and analyzed for the impact of future grid impedance with high penetration of distributed generation and improved LVRT ability of the system in [34]. In [35], [36] an additional cascading converter topology has been proposed to mitigate the stator flux oscillation of DFIG and to enhance the LVRT and HVRT capabilities in dynamic conditions.

In [36], the application of PSS, SVC, and STATCOM devices for improving SS and transient stability is discussed and a robust method based on Particle Swarm Optimization (PSO) is proposed for optimizing parameters of their controllers. In [37], a comparison of PSS, SVC and STATCOM controllers regarding damping interarea oscillations has been described. The combined application of PSS and SSSC is described in [38] for enhancing the transient and small signal stability and in [29] for improving the transient stability and LVRT capability of a power system with RERS.

The coordination of PSS and FACTS thyristor controlled series capacitor (TCSC) damping controllers was explained

in paper [27] to enhance the SS stability of large-scale power systems. In research [39], the effect of PSS and TCSC on instabilities related to Hopf Bifurcation (HB) has been analyzed. The authors have suggested that a coordinated control of PSS and the TCSC may delay the point of HB as compared to the case when the PSS is acting alone in the system. A new coordinated design between PSSs and a unified power flow controller (UPFC) is proposed in [40] for damping local and interarea modes of oscillations by using genetic algorithm (GA). The combined interaction of a unified power quality conditioner and superconducting magnetic energy storage is proposed to enhance the LVRT of DGIG and the permanent magnet synchronous generator. The effectiveness of the proposed technique is verified during fault conditions and wind speed variation [41]. The literature [42] discusses the application of PSSs and the generalized UPFC-power oscillation damping (GUPFC-POD) in a multimachine power system and proposes a technique based on the novel bat algorithm (NBA) for the parameter design of these devices for enhancing SS stability.

The combined use of SFCL and STATCOM and the combined use of resistive-type SFCL and UPFC has been discussed in [43] and [44] respectively for improving the transient stability of a multi-machine power system.

This paper discusses the stability enhancement of an induction generator (IG) based wind power generation system (WPGS). The combined use of PSSs, FCLs and FACTs devices for stability enhancement is increasing worldwide as the traditional power grid is becoming a Smart Grid with the integration of DG based on renewable energy resources (RERs). Damping of generator rotor oscillations is obtained by PSS with the help of excitation controllers on the basis of auxiliary stabilizing signals. The delta Power PSS which is most efficient than other PSSs is selected for the test system.

For improving the rotor angle and the frequency stability, resistive superconductor fault current limiter (R-SFCL) is used. Two indices, namely, transient stability index and sum of maximum deviations (SMD) index are introduced for determining the optimal locations of different sized R-SFCLs for enhancing the rotor angle stability. For increasing the frequency stability, sensitivity index is used and the optimal locations of different sized R-SFCLs is determined on the basis of power change between areas by utilizing sensitivity index (SI). It is important to determine optimal location of R-SFCL considering all stability types; otherwise, R-SFCL will only improve the transient stability of the system in case of a fault at other locations of the system. Along with rotor angle and frequency stability, LVRT capability improvement of a wind farm using STATCOM is also considered. Moreover, combined effect of STATCOM and R-SFCL on rotor angle and frequency stability for different fault locations is also investigated for determining optimal location of R-SFCL to enhance the overall stability of the system. In contrast to the existing literature, this paper considers the improvement in rotor-angle and frequency stability, and LVRT capability of a power system by using three components, namely, PSS, R-SFCL and STATCOM. The results presented in the paper show that STATCOM affects both the number of feasible locations and the optimal locations that can be selected for different sized R-SFCLs of the system for improving the rotor angle and frequency stability during faults. Moreover, it is pointed out that an optimal combination between the different sizes and the locations of R-SFCLs and STATCOM exists in order to enhance the overall stability of the test system under fault conditions. Keeping in view the increasing number of power networks which incorporate PSSs, R-SFCL and FACTS devices jointly, it is important to consider the mutual interaction of these devices for the selection of optimal loaction of R-SFCL for enhancing the system's overall stability. This topic according to the best of the author's knowledge is not so far covered in the existing literature.

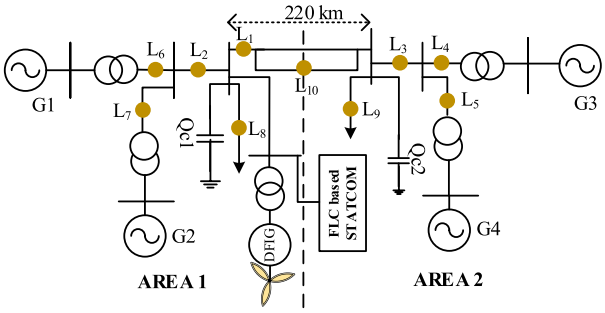

FIGURE 1. IEEE benchmarked four-machine two-area test system.

The rest of this paper is organized as follows: the test system's description is given in section II. Different methods used to improve rotor angle and frequency stability, and their mathematical expressions are described in section III. Fuzzy Logic Controller (FLC) based STATCOM controller design is also discussed in section III. The results and their analysis is given in section IV. The section V, finally, concludes the paper.

II. THE CASE STUDY

Fig. 1 is the single line diagram of the IEEE benchmark four machine two area test system used for the case study. The details of system are given in appendix in table 13 to table 21 [45]. All the test system generators are equipped with power system stabilizers to improve the small signal stability. An R-SFCL is used to improve the rotor angle and frequency stability, and ten different locations are considered for the optimal application of R-SFCL as shown in Fig. 1. An IG based wind power generation system (WPGS) with a total capacity of 9 MVA is integrated into the area 1. A 9 MVA STATCOM is also attached at area 1 to enhance LVRT of the IG based WPGS [46].

III. METHODOLOGY

To analyze the stability of system, various indices have been proposed. Mathematical basis for the stability indices and the methodology to improve the system stability and LVRT has been discussed in this section.

A. SMALL SIGNAL STABILITY IMPROVEMENT USING PSS

Damping in generator rotor oscillations is obtained by PSS with the help of controlling the excitation of generator on the basis of auxiliary stabilizing signal. The common input signals for PSS include shaft speed, terminal frequency and integral of power. On the basis of input signal, PSS has the following types:

- Delta ω PSS
- Delta Pa PSS
- Multi-band PSS
- Frequency-based Stabilizer

As name describes, delta ω PSS has turbine speed as stabilizing signal, delta Pa PSS has turbine power as stabilizing signal, multi-band PSS has both turbine speed and turbine power as stabilizing signal, and frequency-based stabilizer has terminal frequency as stabilizing signal.

B. ROTOR ANGLE STABILITY

When a fault occurs in the network, each generator's rotor angle deviates from its nominal value. Stability can be improved by reducing these rotor angle deviations. R-SFCL has been deployed to damp the rotor angle deviations in case of fault. To find out the deviations, an index is calculated based on the sum of mean deviations (SMD) for all machines with reference to the slack bus. System stability is assessed and enhanced based on this value of SMD and Transient Stability Index (TSI).

The above indices are calculated as:

$$\Delta_{i4} = \delta_{i4}^{MAX} - \delta_{i4}^{MIN} \tag{1}$$

$$\Delta_k = \sum_{i=1}^{3} \Delta_{i4} \tag{2}$$

$$SMD_m = \sum_{i=1}^{N} \Delta_k \tag{3}$$

Where

$m = R\text{-}SFCL\ location\ in\ the\ network$

$k = Fault\ location\ in\ the\ network$

$N = The\ number\ of\ fault\ locations\ investigated$

By introducing R-SFCL, if there is a reduction in the SMD, then it indicates an improvement in the system stability. The Transient Stability Index (TSI) which depends on SMD and resistance of the R-SFCL is calculated as:

$$TSI_m = \frac{\partial SMD_m}{\partial (R - SFCL)} \tag{4}$$

Note that the positive value of TSI_m indicates that the R-SFCL reduces the rotor angle deviations due to which the transient stability of the system increases during a fault. While the negative value of TSI_m indicates that stability is degraded and R-SFCL location is non-optimal. So the best location of R-SFCL is when the TSI_m is maximum for selected resistive value of R-SFCL. The flow chart in Fig. 2 shows the procedure to select optimal location of R-SFCL on the basis of TSI.

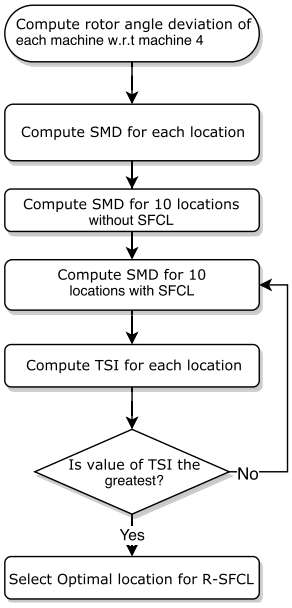

FIGURE 2. Procedure to select the optimal location of the R-SFCL on basis of TSI.

C. FREQUENCY STABILITY

Frequency stability of the system is improved by damping frequency oscillations. This is accomplished by reducingpower change between areas with the help of R-SFCL. Optimal location and optimal resistive value of R-SFCL for frequency stability is determined on the basis of sensitivity index (SI).

For optimal location of the R-SFCL, a new index is used [21].

$$PCA = \left| \int_{0s}^{t_f} (P_{transmission}^{scheduled} - P_{transient}) \right| \tag{5}$$

where

$PCA = Power\ change\ between\ areas$

$P^{Scheduled}$ is the nominal power flow in steady state, i.e, 413.3 MW and t_f is the settling time after clearing the fault and is taken as 20s.

Sensitivity index based on PCA is defined as:

$$SI = \sum_{fault-case} \frac{\partial PCA}{\partial (R - SFCL)} |_{Location} \tag{6}$$

The flow chart in Fig. 3 shows the procedure to select the optimal location of R-SFCL.

D. LVRT CAPABILITY IMPROVEMENT USING STATCOM

During the fault, voltage dip occurs at the generator terminals. This voltage dip should be within the specific limits to avoid tripping. By using fuzzy logic controller (FLC) based STATCOM, the voltage dip is improved during the fault. There are two inputs to the FLC of STATCOM that are error (E) and change in error (CE) of voltage signal. Both inputs and the output have seven linguistic variables of the triangular type. So there are forty nine FLC rules as shown in Table 1. Fig. 4 shows the surface of overall developed FLC. Where linguistic variables are negative small (NS), medium negative (MN),

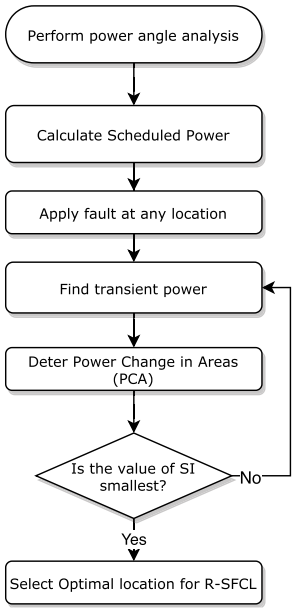

FIGURE 3. Flow chart to select optimal location of the R-SFCL on basis of SI.

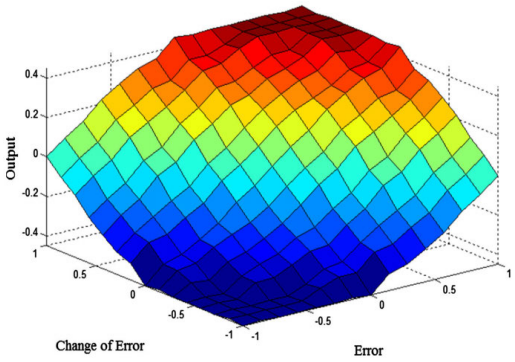

FIGURE 4. Surface of fuzzy logic controller.

TABLE 1. Fuzzy logic controller rules [24].

E	CE						
	BN	MN	SN	Z	SP	MP	BP
BN	BN	BN	BN	BN	MN	SN	Z
MN	BN	BN	BN	MN	SN	Z	SP
SN	BN	BN	MN	SN	Z	SP	MP
Z	BN	MN	SN	Z	SP	MP	BP
SP	MN	SN	Z	SP	MP	BP	BP
MP	SN	Z	SP	MP	BP	BP	BP
BP	Z	SP	MP	BP	BP	BP	BP

big negative (BN), zero (Z), small positive (SP), medium positive (MP), big positive (BP) values respectively.

The STATCOM controller keeps the fundamental voltage component of a voltage-sourced converter (VSC) in phase with the line voltage at PCC during SS conditions. When VSC voltage is not in phase with line voltage, then STATCOM exchanges reactive power corresponding to an error between VSC and line voltage. The magnitude of reactive power exchange depends on transformer leakage reactance (X_{tr}),the magnitude of VSC voltage and the angle. The VSC voltage angle (θ_2)which is normally kept close to zero is temporarily phase-shifted according to the reactive power requirement of the system. The reactive power being delivered or absorbed by the STATCOM is given by Eq. 7.

$$Q_c = \frac{V^2{}_1}{X_{tr}} - \frac{V_1 V_2}{X_{tr}} \cos(\theta_1 - \theta_2) \tag{7}$$

The reactive power exchange between PCC and STATCOM is Q_c. V_1 is the line voltage and V_2 is the STATCOM output voltage. The SS performance model can be written as:

$$Q_c = \frac{V_1^2 - V_1 V_2}{X_{tr}} \tag{8}$$

The size of the compensation devices depending upon the voltage improvement index and the ratio of STATCOM size (Q_{ST}) to the maximum possible STATCOM size ($Q_{ST\,\max}$). The voltage improvement index of the power system is defined as the deviation of the voltage from unity at a bus. The system voltage improvement index (D_v) is written as:

$$D_v = \sqrt{\sum_i^n \left(\frac{V_{iref} - V_i}{V_{iref}}\right)} \tag{9}$$

No. of bus represents n, V_{iref} is the nominal voltage at reference ith bus and V_i denoted the actual voltage at ith bus. The bus voltage must remain in allowable limit between $\pm$ 10 % of the minimal voltage bus voltage. The optimal size of the compensation device is determined from the equation 10 [47].

$$Min\{f(x)\} = Min\{m_1\left(\frac{P_{loss}}{\sum \Delta Loss_{base}}\right) + \{m_2\left(\frac{D_v}{\sum \Delta V_{base}}\right) + m_3\left(\frac{Q_{ST}}{\sum Q_{ST\,\max}}\right) \tag{10}$$

$$m_1 + m_2 + m_3 = 1 \tag{11}$$

$$0 < m_1,\ m_2,\ m_3 < 1 \tag{12}$$

where P_{loss}, $\Delta Loss_{base}$, m_1, m_2 and m_3 are active power loss of the network, base system active power loss and coefficients whose values are determined from the above equations.

IV. RESULTS AND DISCUSSION

In table 2, faults are simulated at 10 different locations and calculated the SMD values for three different types of PSS with and without induction generator (IG) based distributed generation (DG). The table illustrated that Δ (Pa) PSS generated a minimum SMD value of 1270.5 as compared to the other types of PSS. Δ(Pa) is selected further for the test system and tuned parameters of three types of PSS are given appendix. The simulation model has been developed in simulink software to compute δ_{14}, δ_{24}, δ_{34} with a total time of 20s as shown in Figs. 5, 6 and 7 respectively. The plot of δ_{14} reaches its steady state value of 31 within 15.5s. The plot of δ_{24} its steady state value of 22.38 within 14.5s. The plot of δ_{34} reaches its steady state value of 9.5 within 15.5s. The small deviation in δ_{34} is due to the fact that the generators 3 and 4 are located in the same area. This is called local area oscillation. The δ_{14} and δ_{24} have higher values as they belong to inter-area oscillations. The natural frequency setting of

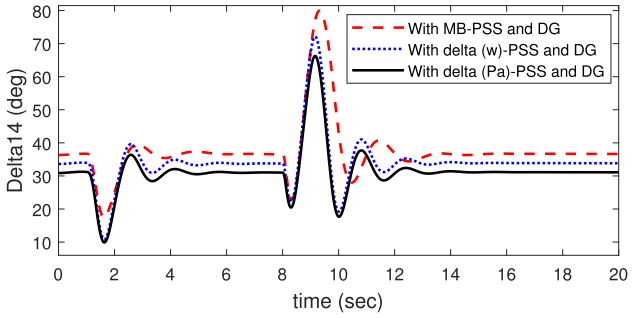

FIGURE 5. Plot of δ_{14}.

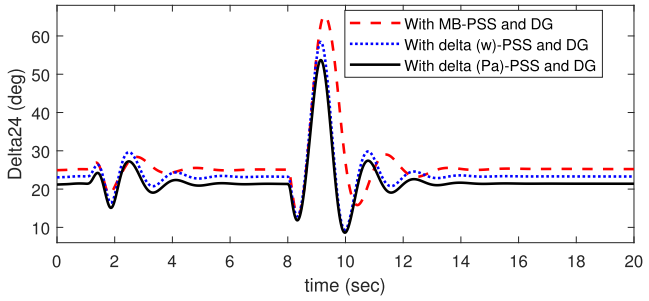

FIGURE 6. Plot of δ_{24}.

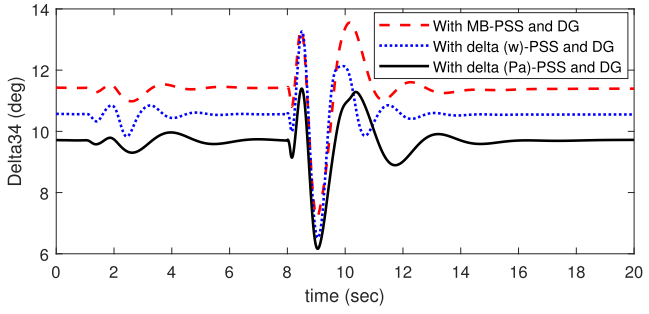

FIGURE 7. Plot of δ_{34}.

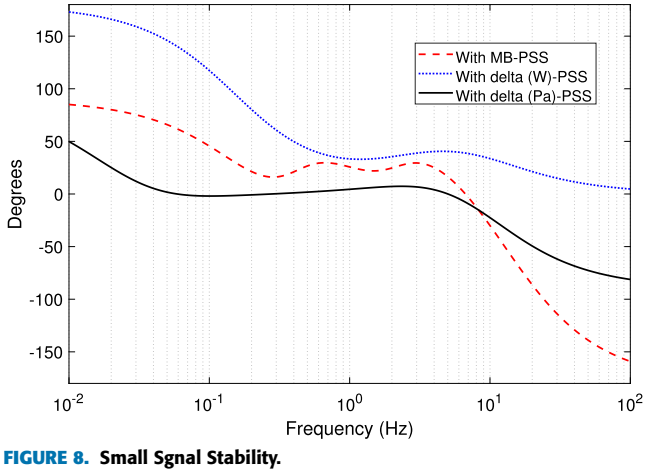

FIGURE 8. Small Signal Stability.

an interarea mode of oscillation is 0.64 Hz. While natural frequency settings of local mode oscillation of Area 1 and Area 2 are 1.12 Hz and 1.16 Hz respectively. In an interarea oscillation mode, Δ (Pa) PSS has a strong combination of phase advance and strong gain at 0.3 Hz as shown in Fig.8 PSS parameters values are given in tables 20 and 21 [45].

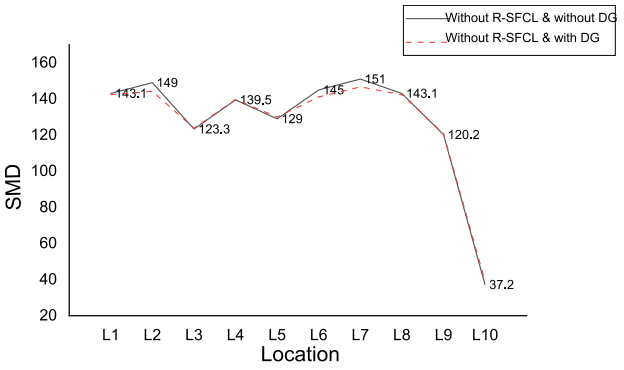

FIGURE 9. SMD for each location without R-SFCL with and without DG.

TABLE 2. SMD for different types of PSS.

Location	No PSS	MB PSS	$\triangle(\omega)$ PSS	$\triangle(P_a)$
L_1	79	141	109	142.4
L_2	82	150	114	144.3
L_3	116	149.4	114	123.8
L_4	88	161	120.5	139.75
L_5	79	141	109	130
L_6	478	132	161	141.15
L_7	3924	156	176	146.7
L_8	3248	140	169	142.4
L_9	582	126	155	120.8
L_{10}	146	38	53	39.2
SMD	8822.5	1333.4	1280	1270.5

A. SMD FOR THE TEST SYSTEM

When a fault is applied to the network, rotor angle deviation can be observed among all generators. In order to stabilize the network, these rotor angle deviations must be reduced to minimum. First of all, SMD is determined without applying R-SFCL. Fig. 9 compares the value of SMD of each fault location without R-SFCL & without DG, and without R-SFCL & with DG respectively. Total value of SMD comes out to be 1280.3 without R-SFCL and without DG and 1270.5s without R-SFCL and with DG.

B. EFFECT OF DIFFERENT TYPES OF POWER SYSTEM STABILIZERS ON SMD

The effect of using different types of PSS is studied for both cases when DG is connected and when DG is not connected. The SMD is very high without PSS and reduces significantly for multi-band PSS. For $\triangle(\omega)$ and $\triangle(P_a)$ PSS, SMD is futher reduced and is minimum for $\triangle(P_a)$ PSS. So, for further simulations, $\triangle(P_a)$ PSS is used. Table 2 shows SMD for ten locations when different types of PSS are used.

C. OPTIMAL LOCATIONS OF DIFFERENT SIZED R-SFCLs USING TRANSIENT STABILITY INDEX

A resistive superconductor fault current limiter (R-SFCL) is employed. Three different values of R-SFCL, i.e., 10 ohm, 20 ohm, and 50 ohm have been considered for the analysis [20] and [21].

TABLE 3. SMD & TSI for each location with R-SFCL=10 ohm.

Location	SMD	TSI	Feasible Location
L_1	1215.2	6.15	Yes
L_2	985.4	29.12	Yes (Best)
L_3	1176.9	9.98	Yes
L_4	1181.9	9.48	Yes
L_5	1257.3	1.94	Yes
L_6	1112	16.47	Yes
L_7	1079.1	19.76	Yes
L_8	1181	9.57	Yes
L_9	1085	19.17	Yes
L_{10}	1302	-2.53	No

TABLE 4. SMD & TSI for each location with R-SFCL=20 ohm.

Location	SMD	TSI	Feasible Location
L_1	1274.8	0.01	Yes
L_2	1075.9	10.04	Yes
L_3	1200	3.84	Yes
L_4	1136.2	7.03	Yes
L_5	1251	1.29	Yes
L_6	992.1	14.23	Yes
L_7	1082.9	9.69	Yes
L_8	1130.8	7.30	Yes
L_9	973.6	15.16	Yes (Best)
L_{10}	1297.4	-1.04	No

1) OPTIMAL LOCATION OF 10 OHM R-SFCL

Table 3 shows the results of SMD and TSI for the case when R-SFCL of 10 ohm is added at each fault location in two area system along with the DG. A three phase fault is considered that lasts for 100 ms, i.e., the fault is applied at 3s and is cleared at 3.1s. The total simulation time is 20s. For R-SFCL = 10 ohm, the optimal location is L_2 as for this location, SMD is the lowest and the value of TSI is the highest. While for location L_{10}, the value of TSI is negative, showing that R-SFCL at this location increases the rotor angle deviations, i.e., it decreases the stability.

2) OPTIMAL LOCATION OF 20 OHM R-SFCL

Table 4 shows the results of SMD and TSI for case when R-SFCL of 20 ohm is added at each fault location in the two area system. For R-SFCL = 20 ohm, the optimal location is L_9 as for this location, SMD is the lowest and value of TSI is the highest. While for location L_{10}, the value of TSI is negative, showing that R-SFCL at this location increases the rotor angle deviations, i.e., it decreases the stability.

3) OPTIMAL LOCATION OF 50 OHM R-SFCL

Table 5 shows the results of SMD and TSI for case when R-SFCL of 50 ohm is added at each fault location in the system under study. For R-SFCL = 50 ohm, the optimal location is L_9 as for this location, SMD is the lowest and value of TSI is the highest. While for location L_1 and L_{10}, the value of TSI is negative, showing that SFCL at these locations increases the rotor angle deviations, i.e., it decreases the stability.

TABLE 5. SMD & TSI for each location with R-SFCL 50 ohm.

Location	SMD	TSI	Feasible Location
L_1	1434.6	-3.15	No
L_2	1125.2	3.03	Yes
L_3	935.8	6.82	Yes
L_4	1035.9	4.82	Yes
L_5	1077.8	3.98	Yes
L_6	937.9	6.77	Yes
L_7	1153.9	2.46	Yes
L_8	1058.5	4.34	Yes
L_9	909.8	7.34	Yes (Best)
L_{10}	1338.6	-1.23	No

TABLE 6. Sensitivity index, PCA and percentage Reduction during the fault at each location with 10 Ω R-SFCL.

Location	*PCA 0* Ω	*PCA 10* Ω	SI R-SFCL: 0 Ω to 10 Ω	Percentage Reduction 10 Ω
L_1	99.7	67.6	-32.1	32.20
L_2	97	43.7	-53.3	54.95
L_3	133.6	62	-71.6	53.59
L_4	161.7	39.7	-122	75.45
L_5	123.4	89.3	-34.1	27.63
L_6	97.6	119.6	22	-22.54
L_7	75.2	144.7	69.5	-92.42
L_8	99.7	136.8	37.1	-37.21
L_9	123.6	0.1134	-123.4866	99.91 (Best)
L_{10}	29.3	16.21	-13.09	44.68

D. OPTIMAL LOCATIONS OF DIFFERENT SIZED R-SFCL USING SENSITIVITY INDEX AND PERCENTAGE REDUCTION

In this case optimal location is determined on basis of sensitivity index which is dependent on power change between areas. Tables 6 and 7 show the results of power change between areas, sensitivity index and percentage reduction in power for the following these three cases.

- When no R-SFCL is added and no DG is connected
- When R-SFCL of 10 ohm is added at each fault location
- When R-SFCL of 20 ohm is added at each fault location

1) OPTIMAL LOCATION OF 10 OHM R-SFCL

The effect of 10 ohm R-SFCL is observed on PCA for each fault location. The R-SFCL is inserted at each fault location and percentage reduction in PCA is observed. Table 6 shows that for locations L_2, L_3, L_4 and L_9, there is significant reduction in PCA and L_9 is the best location. For fault locations L_6, L_7 and L_8, percentage reduction in PCA is negative. This shows that these locations are not suitable for inserting 10 ohm R-SFCL as it reduces the stability.

2) OPTIMAL LOCATION OF 20 OHM R-SFCL

The effect of 20 ohm R-SFCL is observed on PCA for each fault location. The R-SFCL is inserted at each fault

TABLE 7. Sensitivity index, PCA and percentage reduction during the fault at each location with 20Ω R-SFCL.

Location	*PCA 0* Ω	*PCA 20* Ω	SI R-SFCL: 0 Ω to 20 Ω	Percentage Reduction 20 Ω
L_1	99.7	32.8	-66.9	67.10
L_2	97	18.4	-78.6	81.03
L_3	133.6	112.7	-20.9	15.64
L_4	161.7	7.45	-154.25	95.39 (Best)
L_5	123.4	153	29.6	-23.98
L_6	97.6	91.4	-6.2	6.35
L_7	75.2	145.3	70.1	-93.22
L_8	99.7	143	43.3	-43.43
L_9	123.6	53.8	-69.8	56.47
L_{10}	29.3	4.88	-24.42	83.35

TABLE 8. Combined effect of 10 ohm R-SFCL, Δ(Pa) PSS and 9 MVA STATCOM on SMD.

Location	$SMD_{0\ \Omega}$	$SMD_{10\ \Omega}$	Percentage Reduction
L_1	142.4	40.62	71.47 (Best)
L_2	144.3	42.35	70.65
L_3	123.8	74.02	40.21
L_4	139.75	94.32	32.51
L_5	130	121.45	6.58
L_6	141.15	86.24	38.90
L_7	146.7	102.66	30.02
L_8	142.4	58.47	58.94
L_9	120.8	51.87	57.06
L_{10}	39.2	41.54	-5.97

location and percentage reduction in PCA is observed. Table 7 shows that for locations L_1, L_2, L_4, L_9 and L_{10}, there is significant reduction in PCA and L_{10}, there is significant reduction in PCA and L_4 location is the best location. For fault locations L_5, L_7, and L_8, percentage reduction in PCA is negative. This shows that these locations are not suitable for inserting 20 ohm R-SFCL as it reduces the stability.

E. COMBINED EFFECT OF R-SFCL, Δ (Pa) PSS AND STATCOM ON SMD

1) COMBINED EFFECT OF 10 OHM R-SFCL, Δ (Pa) PSS AND 9 MVA STATCOM ON SMD

The effect of 10 ohm R-SFCL and 9 MVA STATCOM is observed on SMD for each fault location. STATCOM is connected to system at point of common coupling (PCC) while R-SFCL is inserted at the each fault location and the percentage reduction in SMD is observed. Table 8 shows that, for locations L_1, L_2, L_8 and L_9, there is significant reduction in SMD and L_1 is the best location. For fault location L_{10}, the percentage reduction in SMD is negative. This shows that the location is not suitable for inserting 10 ohm R-SFCL as it reduces the stability.

TABLE 9. Combined effect of 20 ohm R-SFCL, Δ(Pa) PSS and 9 MVA STATCOM on SMD.

Location	$SMD_{0\Omega}$	$SMD_{20\Omega}$	Percentage Reduction
L_1	142.4	54.2	61.94
L_2	144.3	76.8	46.78
L_3	123.8	94.94	23.31
L_4	139.75	95.62	31.58
L_5	130	155.54	-19.65
L_6	141.15	56.45	60.01
L_7	146.7	115	21.61
L_8	142.4	49.84	65
L_9	120.8	43	64.40 (Best)
L_{10}	39.2	40.4	-3.06

TABLE 10. Sensitivity index, PCA and percentage reduction during the fault at each location with 10 Ω R-SFCL, Δ (Pa) PSS and with 9 MVA STATCOM.

Location	*PCA 0* Ω	*PCA 10* Ω	SI R-SFCL: 0 Ω to 10 Ω	Percentage Reduction 10 Ω
L_1	31.7	89.85	58.15	-183.44
L_2	42.4	113.16	70.76	-166.89
L_3	268.7	81.44	-187.26	69.69
L_4	314	184.2	-129.8	41.34
L_5	285.8	215.25	-70.55	24.69
L_6	44.4	28.82	-15.58	35.09
L_7	64.4	20.5	-43.9	68.17
L_8	31.7	2.33	-29.37	92.65 (Best)
L_9	258.8	140.74	-118.06	45.62
L_{10}	40.43	129.27	88.84	-219.74

2) COMBINED EFFECT OF 20 OHM R-SFCL, Δ (Pa) PSS AND 9 MVA STATCOM ON SMD

The effect of 20 ohm R-SFCL and 9 MVA STATCOM is observed on SMD for each fault location. STATCOM is connected to system at point of common coupling while R-SFCL is inserted at each fault location and the percentage reduction in SMD is observed. Table 9 shows that for locations L_1, L_6, L_8 and L_9, there is significant reduction in SMD and L_9 is the best location. For fault locations L_5 and L_{10}, percentage reduction in SMD is negative. This shows that these locations R-SFCL as it reduces the stability.

F. COMBINED EFFECT OF R-SFCL, Δ (Pa) PSS AND STATCOM ON PCA

1) COMBINED EFFECT OF 10 OHM R-SFCL, Δ (Pa) PSS AND 9 MVA STATCOM ON PCA

The effect of 10 ohm R-SFCL and 9 MVA STATCOM is observed on PCA for each fault location. STATCOM is connected to system at point of common coupling (PCC) while R-SFCL is inserted at each fault location and percentage reduction in PCA is observed. Table 10 shows that for locations L_3, L_4, L_7, L_8 and L_9, there is significant reduction in PCA and L_8 is the best location. For fault locations L_1, L_2 and L_{10}, percentage reduction in PCA is negative. This shows that these locations are not suitable for inserting 10 ohm R-SFCL

TABLE 11. Sensitivity index, PCA and percentage reduction during the fault at each location with 20Ω R-SFCL, Δ (Pa) PSS and with 9 MVA STATCOM.

Location	*PCA* 0 Ω	*PCA* 10 Ω	SI R-SFCL: 0 Ω to 10 Ω	Percentage reduction 10 Ω
L_1	31.7	123.4	91.7	-289.27
L_2	42.4	119.5	77.1	-181.84
L_3	268.7	20.2	-248.5	92.48 (Best)
L_4	314	134.9	-179.1	57.04
L_5	285.8	295	9.2	-3.22
L_6	44.4	53.82	9.42	-21.22
L_7	64.4	25.35	-39.05	60.64
L_8	31.7	14.68	-17.02	53.69
L_9	258.8	61.1	-197.7	76.39
L_{10}	40.43	140	99.57	-246.28

as it reduces the stability. Sections E and G illustrating the interaction of three devices R-SFCLS, Δ(PSS), and STATCOM's impact on SMD and PCA. The simulated results shown in tables 9, 10, and 11 generated the optimal location for R-SFCL.

2) COMBINED EFFECT OF 20 OHM R-SFCL, Δ(Pa) PSS AND 9 MVA STATCOM ON PCA

The effect of 20 ohm R-SFCL and 9 MVA STATCOM is observed on PCA for each fault location. STATCOM is connected to system at point of common coupling while R-SFCL is inserted at each fault location and percentage reduction in PCA is observed. Table 11 shows that for locations L_3, L_4, L_7, L_8 and L_9 there is significant reduction in PCA and L_3 is the best location. For fault locations L_1, L_2, L_5, L_6 and L_{10}, percentage reduction in PCA is negative. This shows that these locations are not suitable for inserting 20 ohm R-SFCL as it reduces the stability.

G. LVRT IMPROVEMENT OF WIND FARM USING STATCOM, PSS AND R-SFCL

FACTS devices including STATCOMs are commonly used to improve LVRT capability of WPGS. For analysis of the LVRT capability, a three-phase short circuit fault is simulated at PCC for 100 msec. It is observed that STATCOM with PSS and R-SFCL has a significant impact on the system performance during fault. A reduction in voltage dips is noted in grid/ system voltage as shown in Fig.10. Thus, the combined interaction of these devices has enhanced the LVRT capability of the IG based WPGS. The values of voltage dips and the percentage improvement IG voltage, and the active power generated by the wind farm are shown in Fig.11 and Fig.12 respectively. The STATCOM's reactive power generation/ absorption in the system dynamic conditions is illustrated in Fig.13. This figure shows that the reactive demand of the system reduces due to the mutual interaction of STATCOM, PSS and R-SFCL.

At the instant of fault, the rotor speed of the IG-based WPGS increases. Resultantly, the pitch angle of the turbine increases to limit the rotor speed to safe limits as is illustrated in Fig.14 and Fig. 15 respectively.

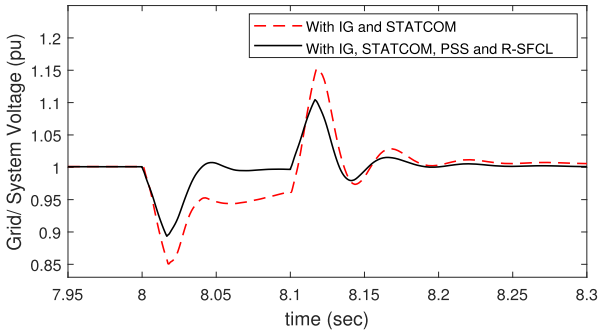

FIGURE 10. Grid/System Voltage in presence of fault at PCC.

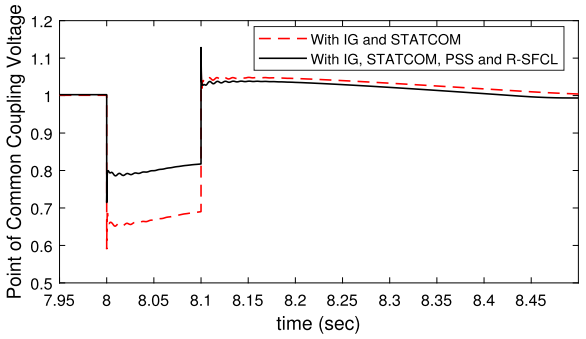

FIGURE 11. Point of common coupling voltage during fault at PCC.

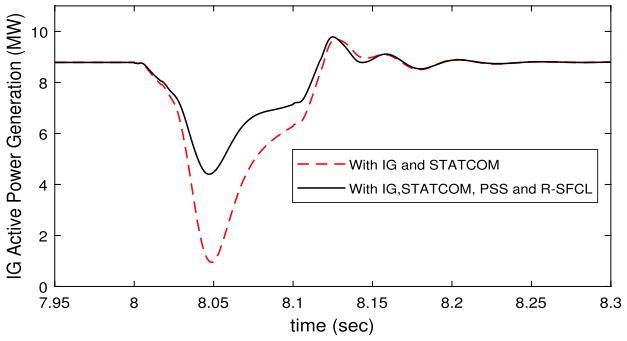

FIGURE 12. Wind farm active power generation in presence of fault at PCC.

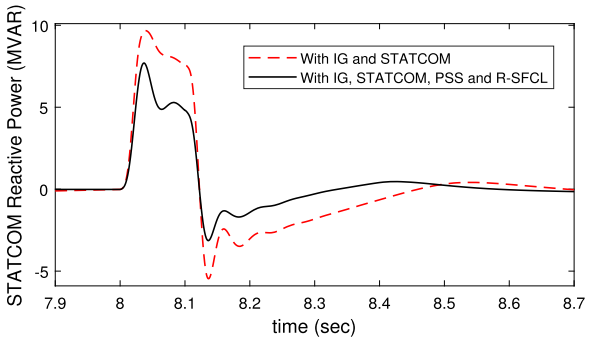

FIGURE 13. STATCOM reactive power response during fault at PCC.

V. FINAL ANALYSIS

On the basis of TSI and SI, the locations L_3-L_9 are feasible for the installation of R-SFCL of 10 Ω in the presence of

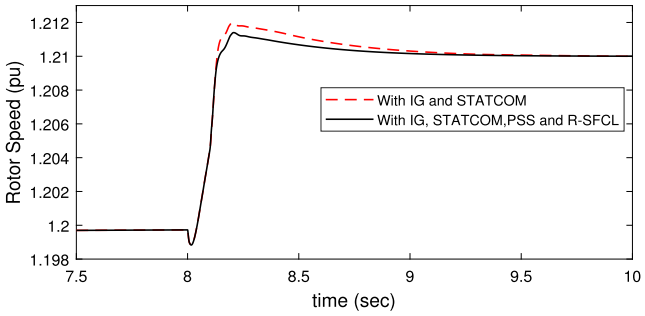

FIGURE 14. Rotor speed during fault at PCC.

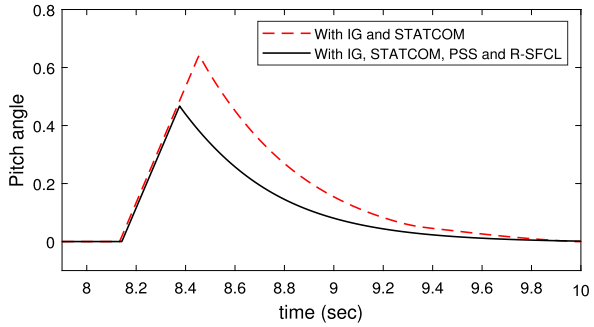

FIGURE 15. Pitch angle during fault at PCC.

TABLE 12. Summary of Feasible Locations Determined on the basis of TSI and SI with Δ (Pa) PSS R-SFCL and STATCOM.

-	*With R-SFCL alone*				With R-SFCL and STATCOM			
R_{SFCL} Size	Feasible Locations Determined on the basis of TSI (SMD)	SI (PCA)	Unsuitable Locations Determined on the basis of TSI (SMD)	SI (PCA)	Feasible Locations Determined on the basis of TSI (SMD)	SI (PCA)	Unsuitable Locations Determined on the basis of TSI (SMD)	SI (PCA)
10Ω	L_1-L_9	L_1-L_5, L_9-L_{10}	L_{10}	L_6- L_8	L_1- L_9	L_3- L_9	L_{10}	L_1-L_2, L_{10}
20Ω	L_1-L_9	L_1-L_4, L_6, L_9-L_{10}	L_{10}	L_5, L_7-L_8	L_1- L_4, L_6- L_9	L_3-L_4, L_7- L_9	L_5, L_{10}	L_1-L_2, L_5- L_6, L_{10}

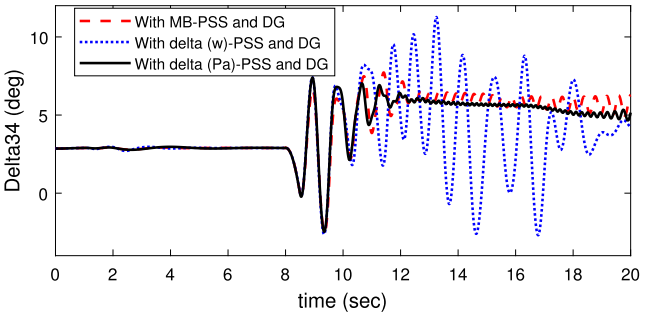

FIGURE 16. Unstable Plot of δ_{34}.

STATCOM as shown in Table 8. Similarly, based on TSI and SI, the locations L_3, L_4 and L_7, L_8, and L_9 are suitable for the installation of 20 Ω R-SFCL in the presence of STATCOM as discribed in Table 10. It is clear that the number of feasible locations for 10 Ω R-SFCL is more than 20 Ω R-SFCL.

Moreover, based on the percentage reduction in SMD, R-SFCL of 10 Ω located on locations L_1 and L_2 give the best results in the presence of STATCOM as shown in Table 8. However, these two locations are unsuitable for the location of R-SFCL based on SI in presence of STATCOM as described in Table 10. Thus, on the basis of Tables 8 and 10, location L_8 is the best option for the installation of 10 Ω R-SFCL. Similarly, on the basis of percentage reduction in SMD, R-SFCL of 20 Ω located at location L_9 gives the best result in the presence of STATCOM as shown in Table 9. However, based on the value of SI in presence of STATCOM as described in Table 11, R-SFCL of 20 Ω located at locations L_3 produces the best results.

On the basis of analysis presented in the paper, it can be noticed that STATCOM affects the number of feasible locations that can be selected for the installation of differently sized R-SFCL in a power network for the minimization of rotor angle deviations (i.e., transient stability) and power exchange between areas during faults, (i.e., frequency stability). Moreover, the analysis presented in the paper also helps to determine the best locations for the connection of different sized R-SFCL in a power network to improve the transient and frequency stability of the system. The results are summarised in Table 12.

The distributed generation based on WPGS of 9 MW capacity is integrated into area 2 at location L_4 and of 18 MW capacity at location L_8 in area 1 without exceeding the stability limit of the system. When the DG penetration level is greater than 27 MW, the system becomes unstable as is described in Fig.16.

VI. CONCLUSION

This paper shows that the rotor angle and frequency stability of a power system can be improved by placing optimally sized R-SFCLs at different location of the network. The optimal locations of different sized R-SFCLs have been determined by using TSI and SMD for increasing the rotor angle stability and by using the sensitivity index (SI) for enhancing the frequency stability. The impact of STATCOM on optimal locations of different sized R-SFCLs has also been discussed in the paper. It is concluded that an optimal combination exists between the different sizes and the locations of R-SFCLs, and STATCOM for augmenting the overall stability of the system during faults.

The proposed strategy may be applied in future to other networks for stability enhancement with a combined application of DFIG based WPGS, nonlinear PSSs, different types of SFCLs and FACTs devices. The comparative analysis of performance of different types of fault current limiters (FCL) for stability improvement in combination with other components is out of the scope of this paper and may be done in the future.

APPENDIX
TEST SYSTEM PARAMETERS

See Tables 13–21.

TABLE 13. Wind Generator Data (IG).

Parameters	Symbol	Values	Parameters	Symbol	Values
Nominal Power	Pn	3/0.9 MVA	Rotor Resistance	Rr	0.004377 pu
Line to line Voltage	Vn	575 V	Rotor Inductance	Lr	0.1791 pu
Frequency	fn	60 Hz	Magnetizing Inductance	Lm	6.77 pu
Stator Resistance	Rs	0.004843 pu	Inertia Constant	H	5.04 s
Stator Inductance	Ls	0.1248 pu	Friction Factor	F	0.01 pu

TABLE 14. Wind turbine data (IG).

Parameters	Symbol	Values	Parameters	Symbol	Values
Nominal Power	Pn	3 MW	Proportional Gain	Kp	5
Base Wind Speed	vbase	9 m/s	Integral Gain	Ki	25
Base Rotational Speed	wrot	1 pu	Max. Pitch Angle	βmax	45 deg
Maximum Power	Pmax	1 pu	Max. Rate of Change of Pitch Angle	(dβ/dt)max	2 deg/sec

TABLE 15. Wind turbine step-up transformer data (IG).

Parameters	Symbol	Values	Parameters	Symbol	Values
Nominal Power	Pn	4 MVA	Winding 2 Resistance	R2	0.025/30 pu
Winding 1 ph-ph Voltage	V1ph-ph	25 kV	Winding 2 Inductance	L2	0.025 pu
Winding 1 Resistance	R1	0.025/30 pu	Frequency	fn	60 Hz
Winding 1 Inductance	L1	0.025 pu	Magnetizing Resistance	Rm	500 pu
Winding 2 ph-ph Voltage	V2ph-ph	575 V	Magnetizing Inductance	Lm	inf

TABLE 16. STATCOM data.

Parameters	Symbol	Values	Parameters	Symbol	Values
Nominal Voltage	Vn	25 kV	Vdc regulator proportional gain	Kp	0.001
Converter Rating	S	3 MVA	Vdc regulator integral gain	Ki	0.020
Droop	D	0.03 pu	Current regulator proportional gain	Kp	0.3
Vac regulator proportional gain	Kp	5	Current regulator integral gain	Ki	10
Vac regulator integral gain	Ki	1000	Current regulator feed forward gain	Kf	0.22

TABLE 17. Synchronous machine data (G1 to G4).

Parameters	Symbol	Values	Parameters	Symbol	Values
Nominal Power	Pn	900 MVA	q-axis Transient Reactance	Xq	0.55 pu
Line to line Voltage	Vn	20 kV	q-axis Steady State Reactance	Xq	1.7 pu
Frequency	fn	60 Hz	Leakage Reactance	XL	0.2 pu
d-axis Sub-transient Reactance	X"d	0.25 pu	Stator Resistance	Rs	0.0025 pu
d-axis Transient Reactance	Xd	0.3 pu	d-axis Open Circuit Transient Time Constant	Tdo	8
d-axis Steady State Reactance	Xd	1.8 pu	d-axis Open Circuit Sub-Transient Time Constant	T"do	0.03
q-axis Sub-transient Reactance	X"q	0.25 pu	q-axis Open Circuit Transient Time Constant	Tqo	0.4

TABLE 18. Transmission line and capacitor bank data.

Parameters	Symbol	Values	Parameters	Symbol	Values
Positive Sequence Resistance	R	0.0529	Zero Sequence Inductance	L0	0.0061
Zero Sequence Resistance	R0	1.61	Positive Sequence Capacitance	C	$8.77488e^{-9}$
Positive Sequence Inductance	L	0.001403183	Zero Sequence Capacitance	C0	$5.25e^{-9}$
Capacitor Bank					
Capacitive reactive power	Qc1	$2e^{8}$	Capacitive reactive power	Qc2	$3.50e^{8}$

TABLE 19. Synchronous machine step-up transformer data.

Parameters	Symbol	Values	Parameters	Symbol	Values
Nominal Power	Pn	900 MVA	Winding 2 Resistance	R2	$1e^{-6}$ pu
Winding 1 ph-ph Voltage	V1ph-ph	20 kV	Winding 2 Inductance	L2	0.15 pu
Winding 1 Resistance	R1	$1e^{-6}$ pu	Frequency	fn	60 Hz
Winding 1 Inductance	L1	0.0 pu	Magnetizing Resistance	Rm	500 pu
Winding 2 ph-ph Voltage	V2ph-ph	230 kV	Magnetizing Inductance	Lm	500 pu

TABLE 20. Multi-band (MB) PSS parameters.

Low Frequency band		inter mediate Frequency band		High Frequency band		Signal limits			
FL (Hz)	KL	FI (Hz)	KI	FH (Hz)	KH	VL (max)	VI (max)	VH (max)	VS (max)
0.2	30	1.25	40	12	160	0.75	0.15	0.15	0.15

TABLE 21. Δ(w) PSS and Δ (Pa) PSS parameters.

Type of PSS	sensor time constant	Gain	Wash out time constant	Lag #1 Time constant		Lag#2 Time constant		Output Limit	
				T num	T dem	T num	T dem	VS min	VS max
Δw PSS	0.015	30	10	0.05	0.02	3	5.4	-0.15	0.15
Δ(Pa) PSS	0.015	3.125	1	0.06	1	0	0	-0.15	0.15

REFERENCES

[1] J. López, E. Gubía, E. Olea, J. Ruiz, and L. Marroyo, "Ride through of wind turbines with doubly fed induction generator under symmetrical voltage dips," *IEEE Trans. Ind. Electron.*, vol. 56, no. 10, pp. 4246–4254, Oct. 2009.

[2] J. Bhukya and V. Mahajan, "Mathematical modelling and stability analysis of PSS for damping LFOs of wind power system," *IET Renew. Power Gener.*, vol. 13, no. 1, pp. 103–115, Jan. 2019.

[3] M. Edrah, K. L. Lo, and O. Anaya-Lara, "Impacts of high penetration of DFIG wind turbines on rotor angle stability of power systems," *IEEE Trans. Sustain. Energy*, vol. 6, no. 3, pp. 759–766, Jul. 2015.

[4] B. Mehta, P. Bhatt, and V. Pandya, "Small signal stability analysis of power systems with DFIG based wind power penetration," *Int. J. Electr. Power Energy Syst.*, vol. 58, pp. 64–74, Jun. 2014.

[5] M. H. Ali, T. Murata, and J. Tamura, "The effect of temperature rise of the fuzzy logic-controlled braking resistors on transient stability," *IEEE Trans. Power Syst.*, vol. 19, no. 2, pp. 1085–1095, May 2004.

[6] M. H. Ali, T. Murata, and J. Tamura, "Influence of communication delay on the performance of fuzzy logic-controlled braking resistor against transient stability," *IEEE Trans. Control Syst. Technol.*, vol. 16, pp. 1232–1241, 2008.

[7] B. C. Sung, D. K. Park, J. W. Park, and T. K. Ko, "Study on a series resistive SFCL to improve power system transient stability: Modeling, simulation, and experimental verification," *IEEE Trans. Ind. Electron.*, vol. 56, no. 7, pp. 2412–2419, Apr. 2009.

[8] Q. Dong, W. T. B. De-Sousa, J. Geng, X. Zhang, H. Zhang, B. Shen, and T. Coombs, "Influences of the resistive SFCL on the incremental power frequency relay of transmission lines," *IEEE Trans. Appl. Supercond.*, vol. 29, no. 2, pp. 1–7, Jan. 2019.

[9] M. A. H. Sadi, "Combined operation of SFCL and optimal reclosing of circuit breakers for power system transient stability enhancement," M.S. dissertation, Dept. Elect. Comput. Eng, Univ. Memphis, Memphis, TN, USA, 2013.

[10] M. A. H. Sadi and M. H. Ali, "Combined operation of SVC and optimal reclosing of circuit breakers for power system transient stability enhancement," *Electr. Power Syst. Res.*, vol. 106, pp. 241–248, Jan. 2014.

[11] M. H. Haque, "Evaluation of first swing stability of a large power system with various FACTS devices," *IEEE Trans. Power Syst.*, vol. 23, no. 3, pp. 1144–1151, Aug. 2008.

[12] N. G. Hingorani and L. Gyugyi, "Shunt compensators: SVC and STATCOM," in *Understanding FACTS: Concepts and Technology of Flexible AC Transmission Systems*, 1st ed. Hoboken, NJ, USA: Wiley, Dec. 1999, pp. 164–176.

[13] M. H. Ali, T. Murata, and J. Tamura, "Transient stability enhancement by fuzzy logic-controlled SMES considering coordination with optimal reclosing of circuit breakers," *IEEE Trans. Power Syst.*, vol. 23, no. 2, pp. 631–640, May 2008.

[14] C. Huang, X. Y. Xiao, Z. Zheng, and Y. Wang, "Cooperative control of SFCL and SMES for protecting PMSG-based WTGs under grid faults," *IEEE Trans. Appl. Supercond.*, vol. 29, no. 2, pp. 1–6, Mar. 2019.

[15] M. A. H. Sadi and M. H. Ali, "Transient stability enhancement by bridge type fault current limiter considering coordination with optimal reclosing of circuit breakers," *Electr. Power Syst. Res.*, vol. 124, pp. 160–172, Jul. 2015.

[16] A. R. Fereidouni, B. Vahidi, and T. H. Mehr, "The impact of solid state fault current limiter on power network with wind-turbine power generation," *IEEE Trans. Smart Grid*, vol. 4, no. 2, pp. 1188–1196, Jun. 2013.

[17] Y. Shirai, M. Mukai, T. Sakamoto, and J. Baba, "Enhancement test of critical clearing time of one-machine infinite bus transmission system by use of SFCL," *IEEE Trans. Appl. Supercond.*, vol. 28, no. 4, pp. 1–5, Jun. 2018.

[18] K. Peddakapu, M. R. Mohamed, M. H. Sulaiman, P. Srinivasarao, and S. Rajasekhar Reddy, "Design and simulation of resistive type SFCL in multi-area power system for enhancing the transient stability," *Phys. C, Supercond. Appl.*, vol. 573, Jun. 2020, Art. no. 1353643.

[19] G. Didier, C. H. Bonnard, T. Lubin, and J. Lévêque, "Comparison between inductive and resistive SFCL in terms of current limitation and power system transient stability," *Electr. Power Syst. Res.*, vol. 125, pp. 150–158, Aug. 2015.

[20] G. Didier, J. Lévêque, and A. Rezzoug, "A novel approach to determine the optimal location of SFCL in electric power grid to improve power system stability," *IEEE Trans. Power Syst.*, vol. 28, no. 2, pp. 978–984, May 2013.

[21] B. C. Sung, D. K. Park, J. W. Park, and T. K. Ko, "Study on optimal location of a resistive SFCL applied to an electric power grid," *IEEE Trans. Appl. Supercond.*, vol. 19, no. 3, pp. 2048–2052, Jun. 2009.

[22] M. R. Islam, M. A. Hossain, J. Hasan, T. K. Roy, and M. A. Sadi, "Double integral sliding mode controller based bridge-type flux-coupling non-superconducting fault current limiter to protect DFIG-based multi-machine power system under transient-state," *Int. J. Electr. Power Energy Syst.*, vol. 142, Nov. 2022, Art. no. 108271.

[23] G. Didier and J. Leveque, "Study of optimal combination between SFCL location and PSS type to improve power system transient stability," *Int. J. Electr. Power Energy Syst.*, vol. 77, pp. 158–165, May 2016.

[24] M. G. Hemeida, H. Rezk, and M. M. Hamada, "A comprehensive comparison of STATCOM versus SVC-based fuzzy controller for stability improvement of wind farm connected to multi-machine power system," *Electr. Eng.*, vol. 100, pp. 935–951, Jun. 2018.

[25] I. N. Muisyo, C. M. Muriithi, and S. I. Kamau, "Enhancing low voltage ride through capability of grid connected DFIG based WECS using WCA-PSO tuned STATCOM controller," *Heliyon*, vol. 8, no. 8, 2022, Art. no. e09999.

[26] R. Bhushan and K. Chatterjee, "Effects of parameter variation in DFIG-based grid connected system with a facts device for small-signal stability analysis," *IET Gener. Transm. Distrib.*, vol. 11, no. 11, pp. 2762–2777, 2017.

[27] C. Li, J. C. Deng, and X. P. Zhang, "Coordinated design and application of robust damping controllers for shunt facts devices to enhance small signal stability of large-scale power systems," *CSEE J. Power Energy Syst.*, vol. 3, no. 4, pp. 399–407, Dec. 2017.

[28] D. Zakiud, J. Zhang, Z. Xu, Y. Zhang, and J. Zhao, "Low voltage and high voltage ride-through technologies for doubly fed induction generator system: Comprehensive review and future trends," *IET Renew. Power Gener.*, vol. 15, no. 3, pp. 614–630, 2021.

[29] A. Movahedi, A. H. Niasar, and G. B. Gharehpetian, "LVRT improvement and transient stability enhancement of power systems based on renewable energy resources using the coordination of SSSC and PSSs controllers," *IET Renew. Power. Gener.*, vol. 13, no. 11, pp. 1849–1860, Aug. 2019.

[30] H. Rezaie and M. H. K. Rahbar, "Enhancing voltage stability and LVRT capability of a wind-integrated power system using a fuzzy-based SVC," *Eng. Sci. Technol., Int. J.*, vol. 22, no. 3, pp. 827–839, 2019.

[31] R. M. M. Pereira, C. M. M. Ferreira, and F. M. Barbosa, "Comparative study of STATCOM and SVC performance on dynamic voltage collapse of an electric power system with wind generation," *IEEE Latin Amer. Trans.*, vol. 12, no. 2, pp. 138–145, Mar. 2014.

[32] C. M. Verrelli, R. Marino, P. Tomei, and G. Damm, "Nonlinear robust coordinated PSS-AVR control for a synchronous generator connected to an infinite bus," *IEEE Trans. Autom. Control*, vol. 67, no. 3, pp. 1414–1422, Mar. 2022.

[33] A. Fathollahi, A. Kargar, and S. Y. Derakhshandeh, "Enhancement of power system transient stability and voltage regulation performance with decentralized synergetic TCSC controller," *Int. J. Electr. Power Energy Syst.*, vol. 135, Feb. 2022, Art. no. 107533.

[34] Z. Din, J. Zhang, Y. Zhu, Z. Xu, and A. E. Naggar, "Impact of grid impedance on LVRT performance of DFIG system with rotor crowbar technology," *IEEE Access*, vol. 7, pp. 127999–128008, 2019.

[35] Z. Din, J. Zhang, Z. Xu, Y. Zhang, and J. Zhao, "Realization of fault ride through for doubly fed induction generator system with cascade converter," *Int. Trans. Electr. Energy Syst.*, vol. 31, no. 3, Mar. 2021, Art. no. e12792.

[36] Z. Din, J. Zhang, J. Zhao, and Y. Jiang, "Doubly fed induction generator with cascade converter for improving dynamic performances," in *Proc. IEEE Energy Convers. Congr. Expo. (ECCE)*, Sep. 2018, pp. 2568–2575.

[37] N. Mithulananthan, C. A. Canizares, J. Reeve, and G. J. Rogers, "Comparison of PSS, SVC, and STATCOM controllers for damping power system oscillations," *IEEE Trans. Power. Syst.*, vol. 18, no. 2, pp. 786–792, May 2003.

[38] J. Bhukya and V. Mahajan, "Optimization of damping controller for PSS and SSSC to improve stability of interconnected system with DFIG based wind farm," *Int. J. Electr. Power Energy Syst.*, vol. 108, pp. 314–335, Jun. 2019.

[39] M. Tripathy and S. Mishra, "Coordinated tuning of PSS and TCSC to improve Hopf bifurcation margin in multimachine power system by a modified bacteria foraging algorithm," *Int. J. Electr. Power Energy Syst.*, vol. 66, pp. 97–109, Mar. 2015.

[40] L. H. Hassan, M. Moghavvemi, H. A. F. Almurib, and K. M. Muttaqi, "A coordinated design of PSSs and UPFC-based stabilizer using genetic algorithm," *IEEE Trans. Ind. Appl.*, vol. 50, no. 5, pp. 2957–2966, Sep. 2014.

[41] J. X. Jin, R. H. Yang, R. T. Zhang, Y. J. Fan, Q. Xie, and X. Y. Chen, "Combined low voltage ride through and power smoothing control for DFIG/PMSG hybrid wind energy conversion system employing a SMES-based AC-DC unified power quality conditioner," *Int. J. Electr. Power Energy Syst.*, vol. 128, Jun. 2021, Art. no. 106733.

[42] E. L. Miotto, P. B. De Araujo, E. De Vargas Fortes, B. R. Gamino, and L. F. B. Martins, "Coordinated tuning of the parameters of PSS and POD controllers using bioinspired algorithms," *IEEE Trans. Ind. Appl.*, vol. 54, no. 4, pp. 3845–3857, Jul. 2018.

[43] B. Mahdad and K. Srairi, "Application of a combined superconducting fault current limiter and STATCOM to enhancement of power system transient stability," *Phys. C, Supercond.*, vol. 495, pp. 160–168, Dec. 2013.

[44] Z. Wang, S. Han, B. Fan, and L. Chen, "Study of resistive SFCL and UPFC for transient behavior enhancement of multi-machine power system," *IETE J. Res.*, vol. 68, no. 1, pp. 108–116, Jan. 2022.

[45] R. Shankar and P. Kundur, "*Power System Stability and Control II*. New York, NY, USA: McGraw-Hill Books, 1994, p. 581.
[46] V. S. K. V. Harish and A. V. Sant, "Grid integration of wind energy conversion systems," in *Alternative Energy Resources: The Way to a Sustainable Modern Society*. Cham, Switzerland: Springer, 2021, pp. 45–66.
[47] F. Shahnia, S. Rajakaruna, and A. Ghosh, *Static Compensators (STATCOMs) in Power Systems*. Singapore: Springer, 2015.

MUHAMMAD SARWAR received the B.Sc. degree in electrical engineering from The Islamia University of Bahawalpur (IUB), Pakistan, in 2014, and the M.S. degree in electrical engineering from the Pakistan Institute of Engineering and Applied Sciences (PIEAS), Islamabad, in 2016. He is currently pursuing the Ph.D. degree in electrical engineering with Iowa State University, Ames, IA, USA.

He was a Lecturer with PIEAS, from 2016 to 2020. His research interests include voltage stability, grid integration of inverter-based resources, application of machine learning in power systems, and dynamic cosimulation of transmission and distribution systems.

MUHAMMAD ARSHED received the B.Sc. degree in electrical engineering from UET Lahore, Pakistan, in 2017, and the M.S. degree in electrical engineering from the Pakistan Institute of Engineering and Applied Sciences, Islamabad, in 2019.

His research interests include the application of renewable energy and FACTS devices in power systems.

BABAR HUSSAIN received the Ph.D. degree in electrical engineering from the University of Southampton, Southampton, U.K., in 2011.

He is currently a Faculty Member with the Department of Electrical Engineering, Pakistan Institute of Engineering and Applied Sciences, and leads the "Energy and Power Systems Research Group." He has authored various papers in academic journals and international conferences, including a book. His main research interests include the grid integration of distributed (renewable) generation, with a focus on protection, stability, and power quality, FACTS devices, power electronic converters, microgrids, and smart grids.

MUHAMMAD RASHEED received the B.Sc. degree in electrical engineering from IUB, Pakistan, in 2013, and the M.S. degree in electrical engineering from UET, Lahore, in 2017. He is currently pursuing the Ph.D. degree in electrical engineering with the Pakistan Institute of Engineering and Applied Sciences, Islamabad, Pakistan.

His research interests include power system stability and protection, the application of renewable energy, and FACTS devices in power systems.

HANAN TARIQ received the B.S. degree in electrical (power) engineering from COMSATS University, Abbottabad Campus, Pakistan, in 2016, and the M.Sc. degree in electrical engineering from the Imperial College of Business Studies (ICBS), Lahore, Pakistan, in 2018. He is currently pursuing the Ph.D. degree in electrical power engineering with the Gdańsk University of Technology, Poland.

He has been associated with research and teaching at multiple universities, since 2017. His research interests include electrical safety and power system stability and dynamics.

STANISLAW CZAPP (Member, IEEE) received the degree from the Gdańsk University of Technology, Poland, in 1996, and the Ph.D. and D.Sc. degrees, in 2002 and 2010, respectively. He is currently an Associate Professor with the Faculty of Electrical and Control Engineering, Gdańsk University of Technology. He is the author and coauthor of many articles, conference papers, and unpublished studies, such as designs and expert evaluations as well as opinions. He is an expert of the SEP Association of Polish Electrical Engineers in Section 08 electrical installations and devices. His research and teaching activities are related to power systems, electrical installations and devices, electric lighting, and electrical safety.

SARMAD TARIQ received the B.S. degree from Bahauddin Zakariya University (BZU), Pakistan, in 2004, and the M.S. degree in electrical engineering from the Mirpur University of Science and Technology (MUST), Pakistan, in 2012.

He is currently a Deputy Manager with National Transmission and Despatch Company (NTDC), Pakistan. His research interests include power system planning and protection.

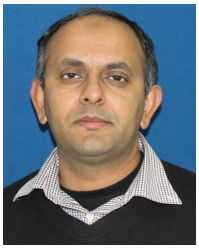

INTISAR ALI SAJJAD (Member, IEEE) received the Ph.D. degree from Politecnico di Torino, Italy, in 2015. He is currently an Assistant Professor with the University of Engineering and Technology, Taxila, Pakistan. He has several publications in IEEE conferences and reputed journals. His research interests include demand-side management and AI applications in PSs.